Applied Catalysis B: Environmental 126 (2012) 144–152

Contents lists available at SciVerse ScienceDirect

Applied Catalysis B: Environmental

journal homepage: www.elsevier.com/locate/apcatb

Local ammonia storage and ammonia inhibition in a monolithic copper-beta zeolite SCR catalyst☆

Xavier Auvray[a], William P. Partridge[b,*], Jae-Soon Choi[b], Josh A. Pihl[b], Aleksey Yezerets[c], Krishna Kamasamudram[c], Neal W. Currier[c], Louise Olsson[a]

[a] Competence Centre for Catalysis, Chalmers University of Technology, Göteborg, Sweden
[b] Fuels, Engines, and Emissions Research Center, Oak Ridge National Laboratory, P.O. Box 2008, MS-6472, Oak Ridge, TN 37831-6472, USA
[c] Cummins Inc., 1900 McKinley Ave, MC 50183, Columbus, IN 47201, USA

ARTICLE INFO

Article history:
Received 24 April 2012
Received in revised form 16 July 2012
Accepted 19 July 2012
Available online 27 July 2012

Keywords:
SCR
Ammonia
NO
NH_3 capacity
NH_3 inhibition
Distributed reactions
Cu-beta
Zeolite

ABSTRACT

Selective catalytic reduction of NO with NH_3 was studied on a Cu-beta zeolite catalyst, with specific focus on the distributed NH_3 capacity utilization and inhibition. In addition, several other relevant catalyst parameter distributions were quantified including the SCR zone, or catalyst region where SCR occurs, and NO and NH_3 oxidation. We show that the full NH_3 capacity (100% coverage) is used within the SCR zone for a range of temperatures. By corollary, unused NH_3 capacity exists downstream of the SCR zone. Consequently, the unused capacity relative to the total capacity is indicative of the portion of the catalyst unused for SCR. Dynamic NH_3 inhibition distributions, which create local transient conversion inflections, are measured. Dynamic inhibition is observed where the gas phase NH_3 and NO concentrations are high, driving rapid NH_3 coverage buildup and SCR. Accordingly, we observe dynamic inhibition at low temperatures and in hydrothermally aged states, but predict its existence very near the catalyst front in higher conversion conditions where we did not specifically monitor its impact. While this paper addresses some general distributed SCR performance parameters including Oxidation and SCR zone, our major new contributions are associated with the NH_3 capacity saturation within the SCR zone and dynamic inhibition distributions and the associated observations. These new insights are relevant to developing accurate models, designs and control strategies for automotive SCR catalyst applications.

1. Introduction

Vehicles are increasingly equipped with diesel or lean-burn engines, which burn fuel in excess air, and which are demanded for their environmental and economical advantages. Specifically, they enable reduced fuel consumption and CO_2 emissions, which is a major greenhouse gas. The oxygen-rich exhaust of such engines make conventional three-way catalysts (TWC) inefficient for the abatement of pollutants such as NO_x ($NO+NO_2$). In Europe and the US, NO_x emission regulations are becoming more restrictive, with EURO and TIER norms, and the automotive industry has made significant efforts developing efficient solutions for converting NO_x to N_2 in such oxygen-rich exhausts.

Two catalytic processes have emerged as promising and applicable for NO_x abatement in oxygen-rich exhaust streams. The NO_x-storage and reduction (NSR) process introduced by Toyota [1] operates in a cyclic mode. During normal operation (excess air) NO_x is oxidized and stored on the NSR catalyst primarily in the form of nitrates [1–3]. To regenerate the catalyst in the second phase of the cyclic NSR process, excess fuel is injected into the engine cylinder during a short period of rich operation. Consequently, the stored NO_x are released and reduced by the reductant-rich exhaust, and the NSR catalyst is then regenerated and able to store NO_x again. Selective catalytic reduction (SCR) is another process, which aims to selectively and continuously reduce NO_x during engine operation. During SCR operation, a reducing compound is continuously injected into the exhaust upstream of the catalyst. Many reductants have been considered and studied including hydrocarbons (HC) [4], CO [5,6], NH_3 [7–11] or even H_2 [6]. Likewise, a range of catalyst materials have been considered for SCR applications; vanadia-based catalysts [10,12,13] and ion-exchanged zeolites [11,14–21] are well-regarded NH_3-SCR catalysts.

☆ *Notice.* This submission was sponsored by a contractor of the United States Government under contract DE-AC05-00OR22725 with the United States Department of Energy. The United States Government retains, and the publisher, by accepting this submission for publication, acknowledges that the United States Government retains, a nonexclusive, paid-up, irrevocable, worldwide license to publish or reproduce the published form of this submission, or allow others to do so, for United States Government purposes.

* Corresponding author. Tel.: +1 865 946 1234.
E-mail address: partridgewp@ornl.gov (W.P. Partridge).

0926-3373/$ – see front matter © 2012 Elsevier B.V. All rights reserved.
http://dx.doi.org/10.1016/j.apcatb.2012.07.019

The catalyst-control challenges, and the choice of SCR catalyst material and reductant vary with application. Using hydrocarbons (HC) as an SCR reductant in automotive applications has the advantage of being available onboard and requiring only a system of injection; however, there is a clear and direct fuel penalty associated with such fuel use. Ammonia–SCR does not directly use fuel for catalyst operation, but necessitates an additional onboard tank and system for storing, dosing and mixing the NH_3 precursor. Such NH_3–SCR systems are used on stationary NO_x sources such as power plants [22] for which supported V_2O_5 based catalysts are very efficient and have been widely studied [13,23,24]. Compared to such stationary applications, automotive NH_3–SCR systems have additional challenges due to their dynamic, mobile and compact nature, and the greater range of operating conditions. Indeed in real driving conditions the amount of NO_x, the NO:NO_2 and temperature all fluctuate, and the NH_3 dosing must vary accordingly. For automotive applications, metal exchanged zeolite-based catalysts are more appropriate because of their high temperature stability; e.g. the SCR catalyst is often positioned downstream of a catalyzed diesel particulate filter which can generate high exhaust temperatures during regeneration. Ammonia storage is significant on NH_3–SCR catalysts, and excess ammonia can be stored on the SCR catalyst and subsequently used to reduce NO_x when the engine operates in conditions producing greater NO_x emissions. Furthermore, catalyst recent history must be incorporated in control strategies as it impacts the amount and distribution of NH_3 stored on the catalyst. These complex, dynamic and distributed factors must be considered in developing ammonia-injection control strategies for optimized performance. The widely varying and interdependent rates of ammonia adsorption/desorption, SCR and other secondary reactions lead to a widely varying and transient reactant conversion and product selectivity [25]; thus models and control strategies based on steady-state analysis are fundamentally limited with respect to optimizing efficiency. Resolution of the distributed chemistry along the monolithic SCR catalyst is highly desired for model development and validation, and for better SCR catalyst and controls design necessary for efficient SCR systems. Specifically, greater insight is needed regarding how NH_3 coverage is distributed along the SCR catalyst and its correlation with distributed SCR reaction. Localized NH_3 inhibition of SCR reactions is particularly relevant to low-temperature and dynamic automotive applications [26], and can further complicate SCR catalyst design and control. Ammonia inhibition has been observed for V [27] and Fe [14,28] SCR catalysts, and is most apparent under dynamic operation conditions typical of engine operation. Global kinetic models [29], as well as a modified redox SCR rate law have been shown to capture the transient SCR performance under dynamic-NH_3-inhibition conditions [14,26–28]. In addition to this dynamic nature, inhibition could furthermore vary the local NH_3 coverage along the catalyst further complicating SCR catalyst design and control. Although NH_3 inhibition is much-less significant and not readily associated with Cu SCR catalysts, it has been observed in steady-state integral measurements over Cu-ZSM-5 catalysts [30–32]. However, dynamic NH_3 inhibition of SCR over Cu catalyst has not been reported. Understanding the distributed NH_3 capacity utilization and inhibition of Cu–SCR catalysts, and how these impact catalyst reactions and performance parameters can provide broadly enabling insights necessary to realize advanced efficiency gains, including better understanding of catalyst reaction details, improved models and development tools, and better control; thus such studies are integral to advancing catalyst efficiency.

In this paper, we provide new information regarding local NH_3 storage and inhibition along the length of a monolithic Cu-beta zeolite SCR catalyst. Specifically, the degree and distribution of NH_3 coverage and inhibition is correlated with the SCR-reaction and species-concentration distributions. These new insights are enabled by transient distributed analysis not previously reported in the literature. To enable the NH_3 storage and inhibition correlations, we first determine SCR reaction distributions, and then use this information to assess the NH_3 impacts at three operation temperatures. The resulting insights have clear relevance to improving SCR models and control.

2. Experimental

2.1. Catalyst

The catalyst used was a Cu-beta zeolite prepared as described in [33,34] and washcoated on a 400-cpsi monolithic cordierite support. The silica-to-alumina ratio was 38 and was prepared using beta zeolite from Zeolyst International. The copper content was 4.3 wt%, measured by inductively coupled plasma and atomic emission spectrometry (ICP-AES). A cylindrical catalyst core sample (25.4-mm long × 7.1-mm diameter) was used for micro reactor analysis. The catalyst was pretreated for 2 h at 500 °C in a gas stream containing 205 ppm NO, 183 ppm NH_3, 10% O_2, 5% H_2O and Ar balance, to simulate exhaust SCR conditions; this treatment ensures sample thermal stability during subsequent experiments.

2.2. Reactor setup and analytical technique

The catalyst core sample was wrapped in fiber glass insulation tape, to minimize gas flow bypassing the catalyst, and placed in a quartz tube positioned in a reactor furnace. Quartz rods were placed in the tube upstream from the catalyst for gas preheating, and downstream to reduce axial temperature gradients within the sample (only ±1 °C over the 25.4-mm long catalyst). Gases were supplied by mass flow controllers and were preheated and mixed before entering the flow reactor in coiled tubing enclosed in a separate preheater furnace. The distance between the preheater and the reactor was small (ca. 20 cm) and all the gases lines were maintained at >200 °C. A K-type thermocouple was inserted in the sample (ca. mid monolith) from the reactor outlet to measure the catalyst internal temperature. Analysis of the intra-catalyst gas composition was performed using SpaciMS (based on a Pfeiffer Prisma QMS 200) developed in the Fuels, Engines and Emissions Research Center at Oak Ridge National Laboratory in a DOE-funded Cooperative Research and Development Agreement (CRADA) with Cummins Inc. [35–39]. Two fused-silica capillaries (Polymicro Technologies, 50-μm I.D., 185-μm O.D., ca. 2-m long) were inserted in the reactor tube from the inlet. They were fixed to a translating system with ca. 32 mm separating the two capillary tips; this allowed one reference capillary to sample the inlet flow, while the second sampled the flow within one channel of the catalyst core, for the full range of capillary translation. The capillaries were connected to a remotely controlled multiport valve, the outlet of which was linked to the mass spectrometer inlet. This system enables rapid switching between the two capillaries to analyze the gas composition either within or before the catalyst. The capillaries were maintained at ca. >200 °C throughout their entire length. The experiment was carried out at the catalyst exit and six target intra-catalyst locations: 1/2, 3/8, 1/4, 3/16, 1/8 and 1/16 of the total monolith length. For the exit measurement, the capillary was actually positioned just inside the catalyst outlet; this allowed exclusive sampling from the measurement catalyst channel and not adjacent channels, which would complicate the analysis due to channel-to-channel performance (e.g. washcoat loading) differences. The m/z ratios monitored were 15 for NH_3, 28 for N_2, 30 for NO, 44 for N_2O, 46 for NO_2 and 84 for Kr; despite these simple signal assignments, there were numerous cross sensitivities which were considered in our analysis.

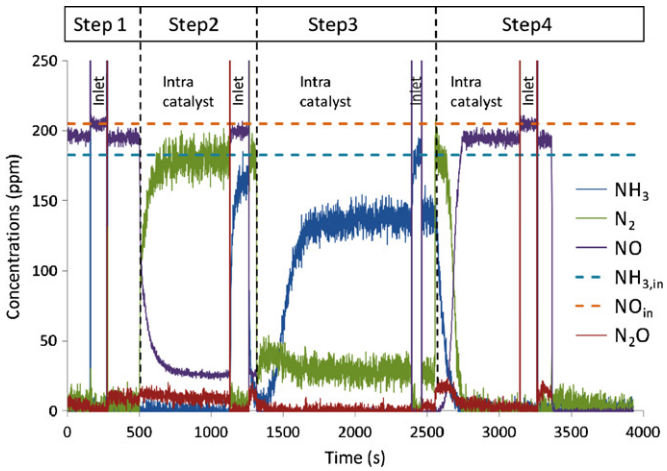

Fig. 1. Transient NO, NH_3, N_2 and N_2O concentrations throughout the 4-step protocol at 0.5L of the catalyst length and 325 °C. Steps 1, 2, 3 and 4 are exposed to NO, NO + NH_3, NH_3, and NO, respectively, at the levels indicated by the dashed lines and correspond to NO oxidation, SCR, NH_3 saturation and cleaning, respectively. The catalyst inlet is samped at the end of each protocol step to verify span concentrations.

2.3. Experimental procedure

The Cummins 4-step protocol [40] was used for analysis and consists of four successive steps at constant flow and temperature:

- Step 1 (NO oxidation): 205 ppm NO, 10% O_2 and 5% H_2O in Ar
- Step 2 (standard SCR): 205 ppm NO, 183 ppm NH_3, 10% O_2 and 5% H_2O in Ar
- Step 3 (NH_3 saturation): 183 ppm NH_3, 10% O_2 and 5% H_2O in Ar
- Step 4 (NO oxidation): 205 ppm NO, 10% O_2 and 5% H_2O in Ar

Trace Kr was incorporated for analytical purposes. The total flow was 510 sccm (0 °C and 760 Torr standard conditions) providing a space velocity of 30,000 h^{-1}. Programmable valves were used to switch between the various protocol-step gas compositions. The sample inlet gas was monitored at the end of each step after reaching steady state for analytical purposes. To assess repeatability, the 4-step protocol was repeated twice at each location and temperature, and the second was used for analysis. The catalyst nature was studied at 200 °C, 325 °C and 400 °C.

Ammonia oxidation (Step3) and SCR conversion (Step2) distributions were used to verify the intended intra-catalyst sampling locations relative to the catalyst inlet. Ammonia oxidation was used for the 325 and 400 °C cases. At 325 °C, the front four points of the ammonia oxidation distribution were ca. linear and used to estimate the actual catalyst inlet, resulting in a spatial correction of +0.018L. At 400 °C the first intra-catalyst position showed no conversion and the inlet position was thus assumed to be −1/16L. At 200 °C, the same offset (−1/16/L) was used based on zero SCR conversion at the first position and the ca. linear conversion distribution throughout.

3. Results and discussion

Fig. 1 shows the four-step protocol results at 325 °C and 0.5L, and how the inlet gas is sampled for a short time in each step after reaching steady state. A small amount of NO oxidation is apparent in Step 1 during NO, O_2 and H_2O feed. During Step 2 SCR, the steady-state NH_3 conversion is 100%, N_2 reaches ca. 170 ppm, and only a minor amount of N_2O is observed. Further, steady-state NO is observed due to the sub-stoichiometric NH_3/NO feed ratio (183 ppm NH_3 versus 205 ppm NO).

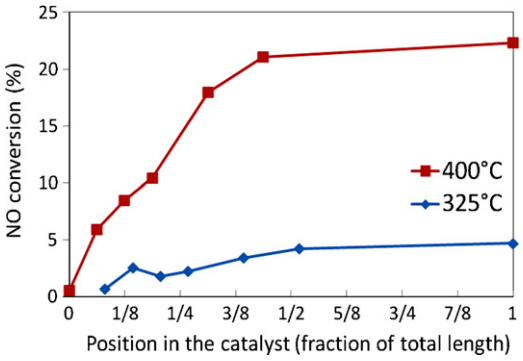

Fig. 2. Axial distribution of NO oxidation from Step 1 of the four-step protocol at 325 and 400 °C.

It is apparent from the Step 2 inlet sampling section of Fig. 1, that co-flowing NO degrades the MS NH_3 response. Specifically, based on 18 independent measurements (at 6 catalyst locations and 3 temperatures), the average measured NH_3 concentration with co-flowing NO (Step 2) was 169 ppm (ca. ±3%) compared to the actual flowing 183 ppm NH_3. This effect was taken into account when calculating the NH_3 conversion in the SCR step (Step 2) by use of a multiplicative factor determined as the ratio between the known and measured inlet NH_3 concentration.

Steady state NH_3 oxidation and corresponding N_2 production are apparent in Fig. 1, Step 3 (NH_3 saturation), when NO is turned off and the feed consists of only NH_3, O_2 and H_2O; no N_2O production is observed at these conditions. Step 4 cleans the surface of ammonia (same as Step 1) and prepares the sample for a second protocol cycle. In addition to this steady state conversion information, NH_3 inhibition and dynamic capacity, unused capacity and total capacity are determined from analysis of the transient regions of Steps 2, 3 and 4, respectively, as will be discussed later.

3.1. NO and NH_3 oxidation

Oxidation of NO to NO_2 is of importance to the SCR reaction since it is well known that the NO_2/NO_x ratio greatly influences the mechanism and rate of NH_3 SCR [7,41]. Fig. 2 shows the (Step 1) steady state NO-oxidation conversion distributions at 325 and 400 °C; zero NO oxidation was observed at 200 °C. Although the thermodynamic equilibrium level of NO conversion to NO_2 at 200 °C is 98.9%, zero NO_2 was measured at this temperature due to kinetic limitations. Fig. 2 also reflects NO_2 formation, in that simultaneous NO_2 measurements indicate a total nitrogen balance within 99% (results not shown here). Progressive NO oxidation occurs in the front half at 325 °C to a maximum of ca. 5% conversion at the catalyst outlet, which is far from the equilibrium level of 80.4%. In contrast, NO oxidation is much greater (22% max. conversion) at 400 °C, increases approximately linearly within the first half and then levels off at a value below thermodynamic equilibrium (52.7%). There are several reasons that NO oxidation levels off before reaching equilibrium. Metkar et al. [42] observed that NO_2 inhibits NO oxidation, and higher NO_2 along the catalyst length would progressively decrease the NO oxidation rate accordingly. In addition, the NO oxidation rate can be expected to progressively slow as equilibrium is approached due to the increasing rate of the reverse reaction (NO_2 dissociation).

It is useful to assess NO_x-free NH_3 oxidation with respect to that under SCR conditions, or parasitic NH_3 oxidation, which can limit SCR conversion. Steady state NO_x-free NH_3 oxidation is apparent in Step 3 of Fig. 1 with stoichiometric (2:1, NH_3:N_2) N_2 and zero N_2O production. Fig. 3 shows the steady state NO_x-free NH_3 oxidation distributions at 325 °C and 400 °C; the average NH_3:N_2 ratio

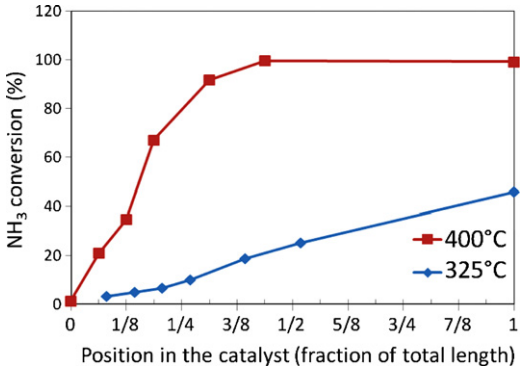

Fig. 3. Axial distribution of NH_3 oxidation from Step 3 of the four-step protocol at 325 and 400 °C.

over the various sampling locations was close to the stoichiometric value for both these temperatures. As was the case for NO oxidation, there was zero NH_3 oxidation at 200 °C. Substantial, linearly distributed, NO_x-free NH_3 oxidation occurs at 325 °C, with a maximum 45% conversion at the catalyst outlet. Ammonia oxidation is even more significant at 400 °C, although still linearly distributed, but complete by the catalyst 0.5L location.

3.2. Ammonia SCR

Figs. 4–6 show the steady state SCR NH_3 and NO conversions in the top panel and the steady state N_2O and N_2 concentrations in the lower panel at 200 °C, 325 °C and 400 °C, respectively. Conversions are listed as NH_3-limited conversion and calculated as the percentage of available NH_3 (183 ppm) owing to the use of substoichiometric NH_3.

At 200 °C (Fig. 4), NO and NH_3 conversions increase linearly within the front half of the catalyst while N_2 and N_2O are simultaneously produced. At this low temperature, 100% conversion is not reached until the back catalyst half. However, 90+% conversion is reached by the 0.5L location. Since measurements were not made between 0.5L and 1L, it is possible that 100% conversion was reached somewhere in the back half before the outlet. Stoichiometric ammonia-limited NO and NH_3 conversions are observed, indicating zero parasitic NH_3 oxidation. Stoichiometric

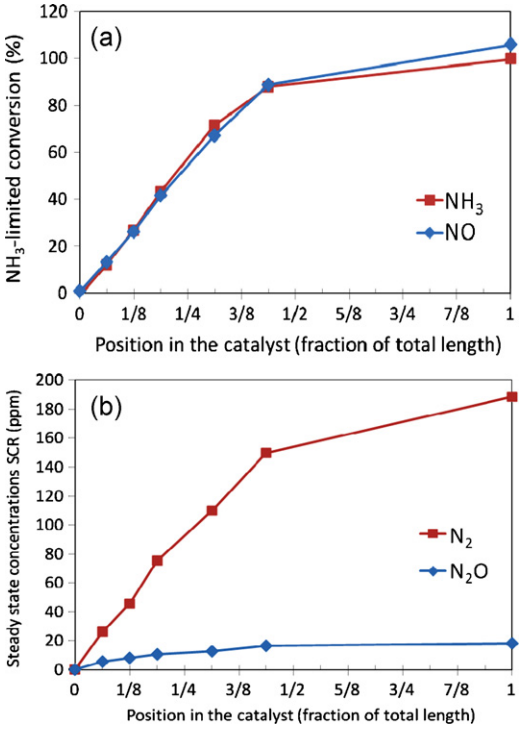

Fig. 4. The steady state SCR activity distributions from Step 2 of the four-step protocol at 200 °C: (a) the NH_3 and NO conversions and (b) the N_2 and N_2O concentrations. NH_3-limited converstions are calculated based on inlet substoichiometric NH_3.

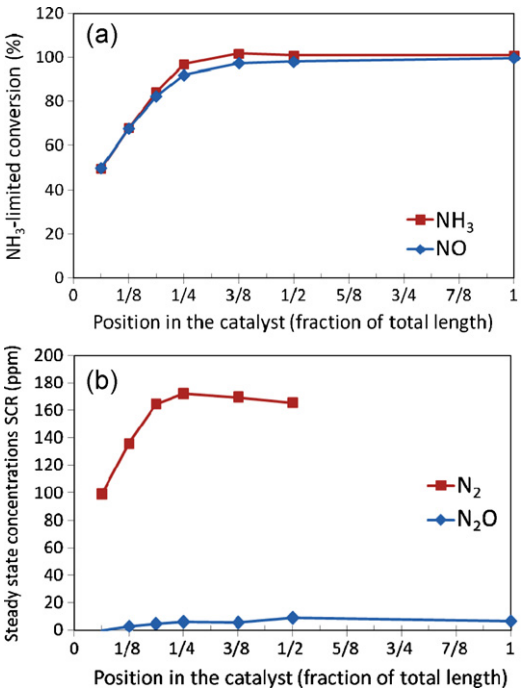

Fig. 5. The steady state SCR activity distributions from Step 2 of the four-step protocol at 325 °C: (a) the NH_3 and NO conversions and (b) the N_2 and N_2O concentrations. NH_3-limited conversions are calculated based on inlet substoichiometric NH_3.

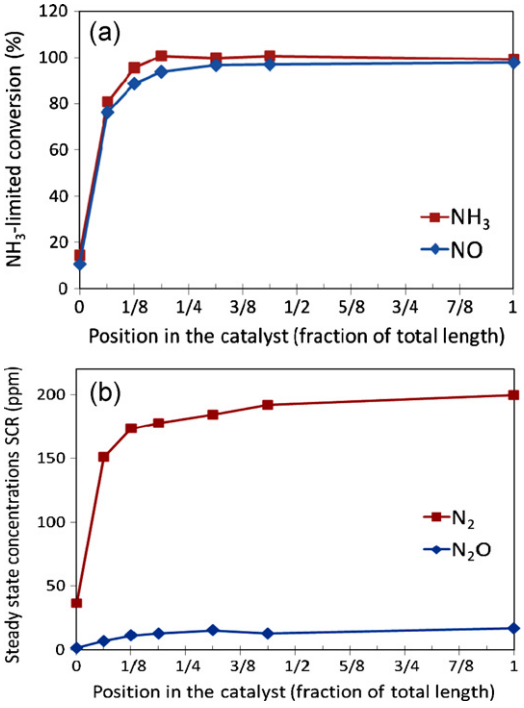

Fig. 6. The steady state SCR activity distributions from Step 2 of the four-step protocol at 400 °C: (a) the NH_3 and NO conversions and (b) the N_2 and N_2O concentrations. NH_3-limited conversions are calculated based on inlet substoichiometric NH_3.

consumption has been observed for several copper zeolites, such as Cu-ZSM5 [32] and Cu-beta [33]. However, for several Fe–zeolite type catalysts an over consumption of ammonia via parasitic oxidation is observed [20,40]. Although only relatively small N_2O concentrations (ca. 18 ppm max) were produced, such levels can be significant in the context of drive-cycle emissions.

At 325 °C, the NH_3 and NO consumption rates, inferred from the initial spatial slopes, are significantly larger than at 200 °C (Figs. 4a and 5a). Thus, less catalyst is required for converting NO and the reaction shifts to the catalyst front. SCR occurs primarily in the front 1/4L, and NH_3 is completely consumed by 3/8L. Notably, the ca. 1:1 NO:NH_3 stoichiometry indicates negligible parasitic NH_3 oxidation under SCR conditions at 325 °C despite significant NO_x-free NH_3 oxidation (Fig. 3), at this temperature. More specifically, this indicates that the SCR reaction is much faster than the NH_3 oxidation reaction at this temperature, and thus high selectivity for the SCR reaction is observed. The N_2 concentration distributions (Fig. 5b) mirror the SCR conversion distributions (Fig. 5a), and the stoichiometry is consistent with the Standard SCR reaction stoichiometry. Delahay et al. [43] observed two modes for N_2O production over Cu–faujasite, one occurring at a low temperature and one at a high temperature. This was also found by Wilken et al. [34] over a Cu-beta, prepared from the same batch of catalyst powder used in this study. According to Centi et al. [44] the N_2O maximum at low temperature is attributed to the formation and decomposition of ammonium nitrates. Further, Delahay et al. [43] suggests that the high temperature N_2O formation originates from reactions on NNN Cu ions located inside the sodalite cages. They were able to reduce this N_2O formation by the introduction of barium. The greater N_2O production at 200 °C compared to 325 °C observed in this study suggests that the dominant N_2O formation pathway under our experimental conditions involved ammonium nitrates.

At 400 °C (Fig. 6), the apparent SCR rate further increases, even less catalyst is required for conversion and the reaction progressively shifts to the catalyst front. Indeed, about 80% conversion is reached by the ca. 1/16L catalyst location. The NH_3 conversion is slightly larger than the NO conversion at 400 °C indicating that the rate for NH_3 oxidation begins to compete with the SCR reaction, resulting in a slightly lower SCR selectivity. However, the SCR selectivity is only affected to a very minor extent, and the 1:1 NO:NH_3 stoichiometry is practically realized. The outlet N_2O concentration was close to 20 ppm, which is larger than that at 325 °C and significant with respect to drive-cycle emissions as mentioned with the similar 200 °C N_2O results. This demonstrates another mode of N_2O formation (high temperature) operating at 400 °C in addition to the low-temperature mode, and which has been reported in the earlier literature [34,43].

A comparison of the SCR NO-conversion distributions throughout the catalyst at the three temperatures investigated is shown in Fig. 7, and highlights the temperature-induced SCR-zone shifts and kinetic differences. Indeed, NH_3 was fully consumed after 1/4L, 3/8L and 1L at 400, 325 and 200 °C, respectively; and the SCR zone variations can be defined accordingly. Although the integral conversion is identical (100%) for the three temperatures, this analysis allows the SCR zone variations to be quantified, which is useful for interpreting NH_3 storage distributions.

3.3. Ammonia storage

Ammonia storage has been observed on Cu-beta [33,34], and various NH_3 capacities can be determined from analysis of the four step protocol transient sections [40] as highlighted in Fig. 8. Specifically, NH_3 capacities are determined from sums of temporal integrals, over the transient protocol sections, of the difference between the instantaneous species concentrations and their

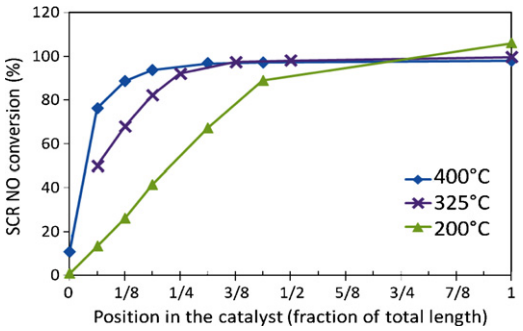

Fig. 7. Spatial profiles of steady state NO conversion during the SCR Step 2 at 200, 325 and 400 °C, showing progressive shift in the SCR zone to the catalyst front with increasing temperature.

corresponding steady state values as described in more detail by Kamasamudram et al. [40]; inherent in this approach is the assumption that oxidation reactions are constant at the steady state value throughout the transient. As Step 2 (SCR) proceeds from an initially NH_3-free catalyst surface, NH_3 is progressively stored on the catalyst as steady state conversion is approached; and in Fig. 8 the SCR reaction becomes increasingly efficient as surface NH_3 coverage increases. Indeed, NO conversion and NH_3 slip are temporally progressive (rather than step like) because of this surface-NH_3 buildup, and indicative of the same. A kinetic model has been developed by Olsson et al. [30] to describe this behavior, which also occurred on Cu-ZSM-5. This surface-NH_3 capacity under SCR conditions, called dynamic capacity (DC), can be calculated [40] from the transient integrals shown in Fig. 8, and may or may not represent the full NH_3 capacity. In cases where the SCR rate is very high it is possible that all ammonia sites are not occupied, because ammonia reacts so fast that a high NH_3 coverage is not achieved. Any unused NH_3 capacity (UC) beyond the DC is filled during Step 3 (NH_3 saturation), and apparent from the transient NH_3 integral shown in Fig. 8. In Step 4 (cleaning the surface of ammonia) NO flows over an initially NH_3-saturated catalyst, and NO reacts with this stored ammonia to form N_2 (and possibly N_2O) via the SCR reaction. The transient approach of NO to its steady state value is indicative of conversion via SCR, and the corresponding surface-NH_3 can be determined from the NO integral shown in Step 4 of Fig. 8; indeed, this can be confirmed from integration of the corresponding N_2 transient. Additional surface NH_3 may desorb

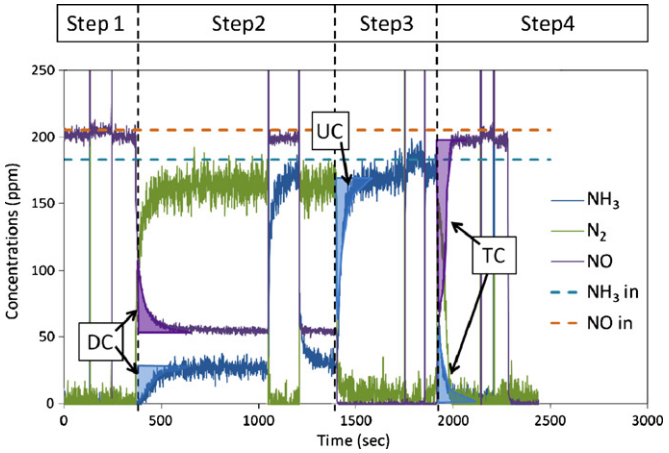

Fig. 8. Transient and steady state NO, NH_3 and N_2 concentration profiles from the four-step protocol, indicating the various NH_3 storage capacities at 3/16L and 325 °C. The capacities are determined from integrating transient regions of the protocol, and the total capacity (TC) is divided into dynamic (DC, that used under SCR conditions) and unused (UC) capacities.

and not be involved in SCR; this portion can be determined from the NH_3 integral shown in Step 4 of Fig. 8. The sum of these Step 4 transient integrals represents the total ammonia capacity (TC). According to Kamasamudram et al. [40], the total NH_3 capacity is the sum of the unused and dynamic capacities (TC = UC + DC).

The NH_3 capacities as shown in Fig. 8 are calculated from the integral of the difference between a step-transient reference and the measured species response. This is practically correct for some species like NO and N_2, which have approximate step instrument response. However, other species like NH_3 and NO_2 have slower non-step-like instrument response; e.g. see the NO and NH_3 responses when switching to the inlet capillary in Step 2 of Fig. 8. Correspondingly, the NH_3-specific instrument response transient should be used in place of the step-transient reference for calculating the portion of the various NH_3 capacities determined from the NH_3 profiles; because the actual NH_3 instrument response is slower than a step reference, this will result in lower integral values. Measurements of the rising and falling NH_3 response during NH_3-span-calibration steps were used to characterize the instrument transient response to corresponding NH_3 steps in the protocol Steps 2 and 4, respectively. The instrument response was extremely repeatable (not shown here) as determined by comparing the normalized rising and falling transient step response for five separate calibrations on different days and at different temperatures. Separate exponential-based fits were determined from these normalized measurements and used to separately characterize the rising and falling NH_3 instrument response. These fits were scaled using the bounding steady state NH_3 values at a specific condition, and used in place of the step function in calculating the NH_3 components of DC and TC. For instance, in determining DC, the fit was scaled using steady state NH_3 value from Step 2. This methodology is a clear improvement over use of step functions in the calculations, and is most correct for applications where the NH_3 transitions are similar to the full-scale span range used for determining the fits; e.g. for TC cases with little Step-3 NH_3 oxidation, and for DC when the Step 2 steady state ammonia concentration is close to 200 ppm. However, at lower Step-2 NH_3 concentrations, such as exist deeper into the SCR zone, the instrument response will likely be slower than described by the fits; this will result in the described methodology overestimating the NH_3 component of the capacity, and thus the overall capacities may be overestimated by some amount. The dynamic and total capacities measured at 200 °C and 325 °C, and calculated using the methods described are presented in Fig. 9a and b, respectively. The NH_3 storage values at 400 °C were very small, and are thus not shown, but followed the same trends discussed for the lower-temperature conditions.

The total capacity distributions shown in Fig. 9 are nominally linear at both 200 and 325 °C. We expect such linear trend, for a catalyst with axially uniform washcoat distribution or loading, assuming that NH_3 stores on some sort of active sites. The TC ranged from 0 to 63 μmol at 200 °C, and from 0 to 19 μmol at 325 °C. The coverage depends on the temperature, and adsorbed NH_3 becomes increasingly unstable at higher temperatures. The maximum storage at 400 °C, observed at the exit, is only ca. 2 μmol (not shown).

As mentioned above, the dynamic capacity reflects the competition between NH_3 storage, surface-NH_3 thermal stability and the SCR reaction. At higher temperatures the surface NH_3 is less stable (cf. TC trends) and the SCR reaction is faster (cf. Fig. 7), both of which could resulting in a smaller DC. Fig. 9 indicates that DC follows the TC in the front of the catalyst and then levels off. Comparing these results to the conversion profiles in Fig. 7, it is apparent that DC increases within the SCR zone only. Beyond the SCR zone, where gas-phase NH_3 is fully consumed, DC can no longer increase, and thus the DC plateaus beyond the SCR zone. The salient point though is that DC practically matches TC within the SCR zone. At 200 °C, SCR occurs in the front half since the NH_3 conversion reaches

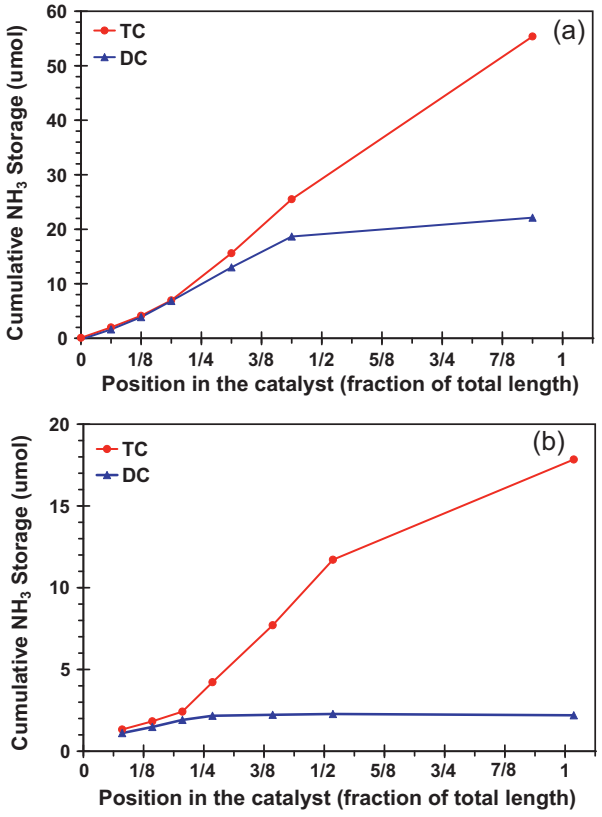

Fig. 9. Total and dynamic NH_3 storage capacity distributions calculated using the results from Step 2 and Step 4 in the four-step protocol at (a) 200 °C and (b) 325 °C, indicating the NH_3 capacity to be practically saturated in the SCR zone; i.e. DC = TC in the SCR zone.

100% by 1/2L; correspondingly at 200 °C DC increases linearly and practically matches TC up to the 1/2L location, and then plateaus. The same correlation is made at 325 °C where SCR and dynamic storage both occur within the front quarter of the catalyst, and DC practically matches TC. Indeed, the same DC:TC correlation exists at 400 °C in the front 1/16L where ca. 80% of the SCR conversion occurs, despite the significantly lower capacity and higher SCR rate at this high temperature. The implication of this observation is that the full NH_3 capacity is used throughout the SCR zone for this catalyst over the full range of temperatures studied (i.e. 200, 325 and 400 °C).

Ammonia storage sites in the post-SCR region cannot be filled during SCR since NH_3 is fully reacted or stored within the SCR zone. However, the NH_3 sites in the post-SCR region are NH_3 free and able to store NH_3 in Step 3 (NH_3 saturation); this additional storage capacity is the UC. A corollary of the conclusion from the preceding paragraph is that UC is zero in the front SCR-region of the catalyst. Thus, UC is indicative of the catalyst portion not used for SCR. Indeed, this could provide valuable catalyst-control insights if methods to quantify UC are available.

The new SCR catalyst insights regarding NH_3 coverage saturation over the SCR zone can be independently corroborated via UC measurements and the capacity balance. The UC distribution is apparent from the spatiotemporal results in Fig. 10, which show the 325 °C NH_3 traces for the 7 intra-catalyst locations at the end of Step 2 (SCR) and throughout Step 3 (NH_3 saturation) until steady state NH_3 is reached. The spatial extent of the SCR region is apparent from the Step-2 tail as the point where NH_3 is fully consumed; this occurs between the ca. 3/16L and 1/4L locations in Fig. 10, which is consistent with Fig. 5a. Within the SCR zone UC is negligible considering the corresponding closely grouped curves in

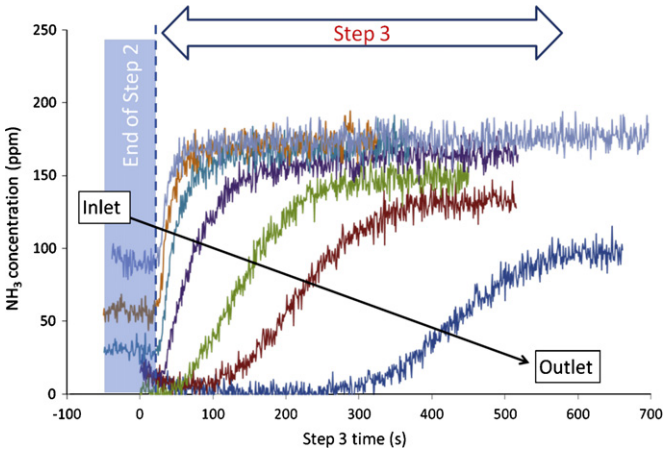

Fig. 10. Unused capacity distributions as evident from the NH_3 concentration traces at the 7 catalyst locations (1/16, 1/8, 3/16, 1/4, 3/8, 1/2, and 1L) from Step 3 in the four-step protocol at 325 °C. Indicates that UC is practically zero in the SCR zone, providing independent corroboration of the Fig. 9b observation indicating DC = TC in the SCR zone.

Fig. 10, and the instrument response differences discussed above. The distinct spreading of the curves in Step 3 downstream of the SCR zone is indicative of UC growth. This supports our observation that UC is zero in the SCR zone and increases in the post-SCR zone. More specifically, along with the capacity balance (TC = DC + UC), this provides independent corroborating evidence that the full NH_3 capacity is used throughout the SCR zone.

3.4. Ammonia inhibition

Catalyst-effluent or integral transient NH_3 inhibition has been observed on V [27] and Fe [14,28] SCR catalysts, and integral steady-state NH_3 inhibition has been observed on Cu-ZSM-5 [30–32]. However, localized and distributed NH_3 inhibition has not been previously reported. This study provides unique opportunity to resolve such localized NH_3 inhibition distributions for gaining further insights into this process. Indeed, NH_3 inhibition is observed at the catalyst front for the 200 °C condition, during initial NH_3 coverage buildup in the transient region of Step 2 SCR. For reference, Fig. 11 shows the spatiotemporal NO and N_2 profiles in this transient region for the front catalyst portions at 325 °C, where dynamic inhibition is not readily apparent. In this case NO conversion and N_2 generation are spatiotemporally progressive with NH_3 coverage buildup. By contrast, dynamic NH_3 inhibition is apparent at the catalyst-front locations in Fig. 12a and b, which shows similar curves for the 200 °C condition. Specifically, the inflections in the 1/16L and 1/8L N_2 and NO profiles are due to inhibition onset caused by the NH_3 coverage reaching a critical threshold. At Step 2 inception, SCR starts from an initially NH_3-free surface. As time progresses NH_3 coverage increases and SCR follows accordingly. The SCR reaction slows as the NH_3 coverage approaches a threshold to cause inhibition, although coverage will continue to increase over time to the steady state DC (=TC as discussed above) value. This SCR slowing causes the conversion rate to slow as apparent at 1/16L and 1/8L in Fig. 12. The further increasing NH_3 coverage causes progressive conversion degradation. This process results in the inhibition-driven conversion inflections apparent in Fig. 12 at the 1/16L and 1/8L locations. A conversion inflection is not apparent in the transient region of the 3/16L curve in Fig. 12 because either slower NH_3 coverage buildup and reaction, or the inhibiting threshold coverage is not reached at that location, as discussed in the following paragraphs. Such inflections indicative of obvious inhibition are not apparent in our measurements at the higher conversion conditions at 325 and 400 °C. However, dynamic

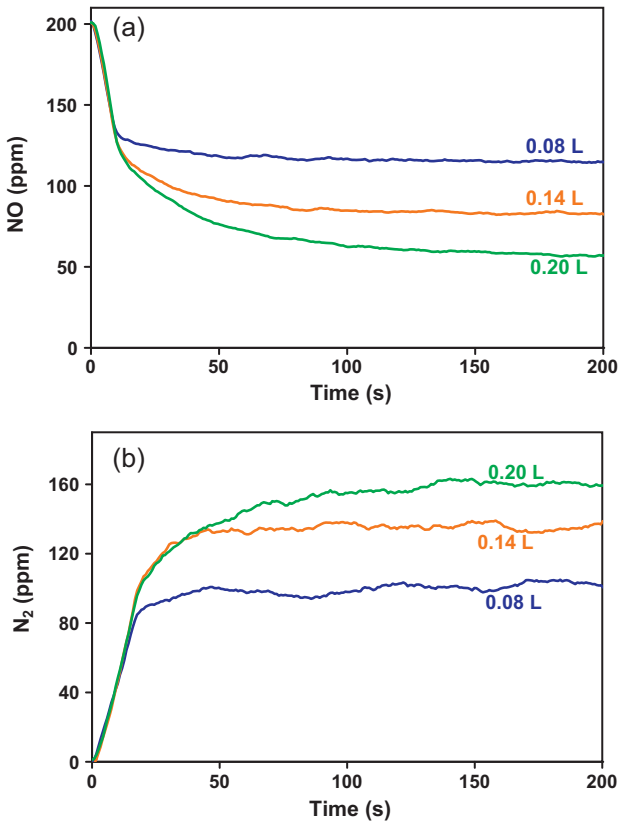

Fig. 11. Transient NO (a) and N_2 (b) profiles at three near-front intra-catalyst locations during the transition to steady-state SCR in Step 2 at 325 °C, indicating monotonically increasing SCR activity typical in the absence of dynamic NH_3 inhibition.

inhibition was apparent at 325 °C with hydrothermal ageing and progressed deeper into the catalyst with progressive ageing; the SCR rate was correspondingly degraded with progressive ageing causing lengthening of the SCR zone (results not shown). Indeed we have consistently observed conversion inflections indicative of dynamic inhibition under conditions where high (ca. >130 ppm for the work here) gas phase NH_3 concentrations (which drive fast coverage buildup) exist; i.e. we have observed such dynamic inhibition at low temperature and hydrothermally aged conditions which allow high gas-phase NH_3 to exist further along the catalyst length due to slower SCR conversion. Based on these observations, it is expected that similar inhibition occurs at the extreme front of the fresh catalyst at 325 and 400 °C as well where such high NH_3 and NO concentrations exist (namely, prior to our first sampling point); i.e. dynamic NH_3 inhibition is expected to occur on this catalyst where the NH_3 coverage buildup rate is suitably high (due to high NH_3). Although such localized dynamic inhibition may not seem significant from an integral steady-state perspective, it impacts adjacent and near-adjacent unit cells within the catalyst, and transient catalyst performance and control so relevant to automotive applications.

Inhibited steady state conditions can be reached without transitioning through a conversion inflection if the temporal NH_3 coverage and NO profiles are sufficiently slow. Although conversion inflections provide dramatic indications of transient NH_3 inhibition, the lack of such inflections deeper into the catalyst do not necessarily indicate an absence of inhibition or inhibition potential. Similarly, the dynamic inhibition distribution strongly biased to the catalyst front apparent in Fig. 12 is not in conflict with the uniform steady state DC distributions over the SCR zone for the same condition (cf. Fig. 9a). Specifically, dynamic inhibition is apparent

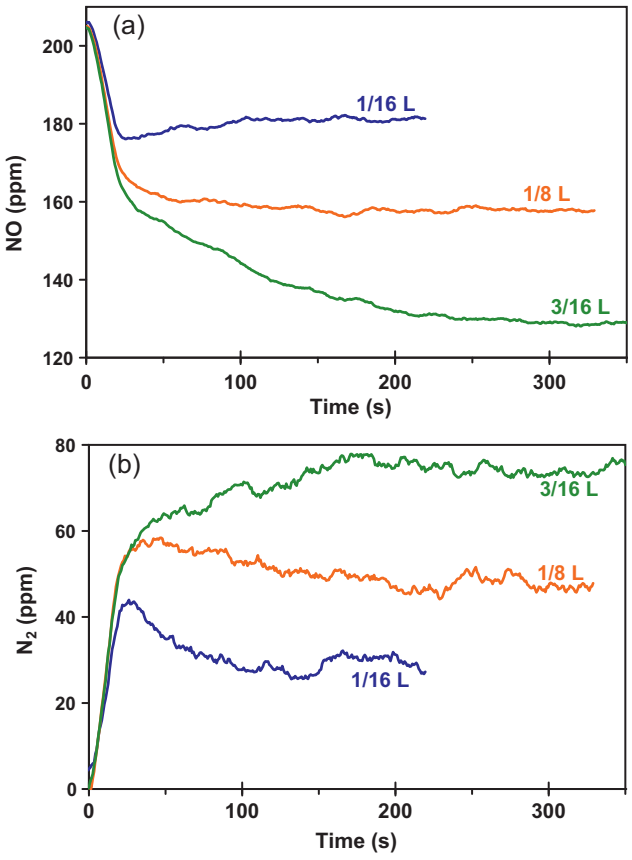

Fig. 12. Dynamic NH_3 inhibition apparent from transient NO (a) and N_2 (b) profiles at three near-front intra-catalyst locations during the transition to steady-state SCR in Step 2 at 200 °C. Conversion inflections at the front two locations indicate dynamic NH_3 inhibition.

at NH_3 coverages below saturation (DC = TC in SCR zone); and thus at steady state the NH_3 coverage appears to be above the threshold necessary to observe dynamic inhibition throughout the SCR zone. Dynamic inhibition may not be apparent deeper into the SCR zone due to the temporal NO and NH_3 coverage profiles; and specifically because the SCR rate is a function of the instantaneous NO concentration and NH_3 coverage [e.g. see the modified redox SCR rate law in [26]], and the temporal NH_3 coverage profile scales with the NH_3 concentration. Generally, NH_3 coverage grows more slowly deeper in the catalyst because the NH_3 concentration is lower, and thus the time and rate to reach the critical NH_3 threshold for inhibition onset is delayed and more gradual; e.g. compare shape of the conversion inflections at the 1/16L and 1/8L locations in Fig. 12. In parallel, the NO concentration is lower deeper into the catalyst, further lowering the SCR rate. Indeed, at sufficiently low NO concentrations, NH_3 inhibition may exist but not be readily apparent. In this way a steady state inhibited SCR condition could be reached without transitioning through a conversion inflection or dynamic inhibition point. Thus, even our 325 and 400 °C degreened steady-state performance may be inhibited despite the lack of temporal inflections. Dynamic NH_3 inhibition requires sufficiently high NO and NH_3 concentrations, which extend further along the catalyst length at lower temperatures and with increasing hydrothermal ageing. Thus dynamic inhibition is observed in these conditions as reported; and expected to exist upstream of our measurement points in the 325 and 400 °C degreened condition where sufficient conditions exist.

An alternate explanation for the lack of conversion inflection at the 3/16L 200 °C case (Fig. 12) is that the inhibiting threshold NH_3 coverage may not have been reached. Indeed, we have shown that the NH_3 coverage is practically saturated over the SCR zone. However, it appears (cf. Figs. 7 and 9) that complete saturation may not occur at the tail end of the SCR zone. And this departure from clear saturation at 200 °C occurs somewhere around the same 3/16L location where dynamic inhibition ceases to be observed. Thus it is possible that DC dropped below the critical coverage threshold for inhibition at the 3/16L location resulting in a lack of conversion inflection; in this case the conversion at that location would not be inhibited. We are working on improved analytical temporal resolution which is needed to elucidate transient SCR, make better DC and TC measurements and resolve the NH_3 capacity buildup to the critical threshold and beyond. Such improved analytical capabilities will allow these fine mechanistic insights regarding inhibition to be resolved.

4. Conclusions

The distributed performance along the length of a monolithic Cu-beta zeolite SCR catalyst was investigated with specific focus on NH_3 capacity utilization and NH_3 inhibition. Inherent to this focus, other catalyst performance measures were quantified including distribution and variation in SCR zone with temperature, NO and NH_3 oxidation. All of these are relevant not just for improving understanding and models of these catalysts, but to their design and control for complex automotive applications.

The general catalyst parameter distributions were initially investigated as a foundation for assessing NH_3 capacity utilization. The SCR reaction occurs in the catalyst front, and the SCR zone shifts progressively to the catalyst front at higher temperatures; the SCR zone was ca. 1L, 3/8L and 1/4L at 200, 325 and 400 °C. This demonstrates how the intra-catalyst SCR gradients and distributions can be very different, despite equivalent (100%) integral performance. Direct (or NO_x-free) NH_3 oxidation was significant at 325 and 400 °C. At 325 °C the NH_3 oxidation increased linearly and reached ca. 40% conversion by the outlet. Direct NH_3 oxidation was much more significant at 400 °C where the conversion was complete midway through the catalyst. Despite such significant NO_x-free NH_3 oxidation, close to 1:1 NO:NH_3 conversion stoichiometry was observed under SCR conditions at 325 and 400 °C. This demonstrates that the SCR reaction is much faster than NH_3 oxidation reactions over this catalyst at the investigated temperature interval.

Ammonia capacity utilization distributions were determined via analysis of the transient protocol sections. In general, the total NH_3 capacity, TC, decreases with increasing temperature as surface-NH_3 stability decreases; and the TC is nominally linearly distributed along the catalyst length as expected. The dynamic NH_3 capacity, DC, is that stored under SCR conditions, and can only exist over the SCR zone where non-zero NH_3 exists. A significant and new insight resulting from this work is that DC is practically equivalent to TC over the SCR zone at 200 and 325 °C; the same trend was observed at 400 °C despite the significantly lower NH_3 capacity and higher SCR rate at that high temperature. This indicates that the full NH_3 capacity is used throughout the SCR region, and that the unused NH_3 capacity, UC, is zero in the same. This observation was independently corroborated by the UC measurement distributions which qualitatively indicated zero UC in the SCR region and growth in the post-SCR region. A consequence of this is that UC is indicative of the catalyst portion not used for SCR. These new insights are applicable to catalyst modeling, design and control.

We demonstrated that dynamic NH_3 inhibition, which creates inflections in the SCR conversion rate, can occur in the catalyst front even when not apparent from integral analysis. Such dynamic inhibition occurs when high NH_3 concentrations are available to drive rapid NH_3 coverage buildup. Thus, dynamic inhibition is apparent

at lower temperatures and with hydrothermal ageing which allow high concentrations to exist further along the catalyst length. Indeed, we observe dynamic inhibition biased to the catalyst front locations at 200 °C; we have also observed similarly biased dynamic inhibition extending progressively further along the catalyst length with increased hydrothermal ageing. Such distributed dynamic inhibition has not been previously reported, and is particularly relevant to dynamic automotive catalyst applications. The fact that the dynamic inhibition has a varying distribution over the SCR zone while the steady state NH_3 coverage distribution is uniform invokes several observations; the onset of the dynamic-inhibition conversion inflection reflects the NH_3 coverage threshold for observing inhibition; in the cases studied here, the steady state coverage is greater than the inhibition threshold; inhibited or potentially inhibited steady-state conditions can be accessed without transitioning through a conversion inflection point; dynamic inhibition requires sufficiently high coverage buildup and SCR; dynamic inhibition may not be observed further along the catalyst length where NH_3 coverage builds up slowly and SCR rates are lower also due to low NO concentrations; dynamic inhibition, while not observed at the sampled points at 325 and 400 °C likely exists where conditions are favorable closer to the catalyst front.

Acknowledgments

This work is a collaboration between Oak Ridge National Laboratory, Competence Centre for Catalysis at Chalmers University and Cummins Inc. This research was sponsored by the U.S. Department of Energy, Office of Energy Efficiency and Renewable Energy, Vehicle Technologies Program, with Ken Howden and Gurpreet Singh as the Program Managers and the Swedish Foundation for Strategic Research (F06-0006).

References

[1] N. Takahashia, H. Shinjoh, T. Iijima, T. Suzuki, K. Yamazaki, K. Yokota, H. Suzuki, N. Miyoshi, S.I. Matsumoto, T. Tanizawa, T. Tanaka, S.S. Tateishi, K. Kasahara, Catalysis Today 27 (1996) 63–69.
[2] E. Fridell, H. Persson, B. Westerberg, L. Olsson, M. Skoglundh, Catalysis Letters 66 (2000) 71–74.
[3] E. Fridell, M. Skoglundh, B. Westerberg, S. Johansson, G. Smedler, Journal of Catalysis 183 (1999) 196–209.
[4] F.C. Meunier, J.P. Breen, V. Zuzaniuk, M. Olsson, J.R.H. Ross, Journal of Catalysis 187 (1999) 493–505.
[5] P.M. Sreekanth, P.G. Smirniotis, Catalysis Letters 122 (2008) 37–42.
[6] M. Haneda, T. Fujitani, H. Hamada, Journal of the Japan Petroleum Institute 49 (2006) 219–230.
[7] A. Grossale, I. Nova, E. Tronconi, D. Chatterjee, M. Weibel, Journal of Catalysis 256 (2008) 312–322.
[8] M. Koebel, M. Elsener, M. Kleemann, Catalysis Today 59 (2000) 335–345.
[9] O. Kröcher, M. Devadas, M. Elsener, A. Wokaun, N. Söger, M. Pfeifer, Y. Demel, L. Mussmann, Applied Catalysis B: Environmental 66 (2006) 208–216.
[10] I. Nova, C. Ciardelli, E. Tronconi, D. Chatterjee, B. Bandl-Konrad, Catalysis Today 114 (2006) 3–12.
[11] M. Colombo, I. Nova, E. Tronconi, Catalysis Today 151 (2010) 223–230.
[12] M.D. Amiridis, I.E. Wachs, G. Deo, J.M. Jehng, D.S. Kim, Journal of Catalysis 161 (1996) 247–253.
[13] J.P. Chen, R.T. Yang, Applied Catalysis A: General 80 (1992) 135–148.
[14] A. Grossale, I. Nova, E. Tronconi, Catalysis Today 136 (2008) 18–27.
[15] G. Cavataio, H.W. Jen, J.R. Warner, J.W. Girard, J.Y. Kim, C.K. Lambert, SAE International Journal of Fuels and Lubricants 1 (2009) 477–487.
[16] T. Cheung, S.K. Bhargava, M. Hobday, K. Foger, Journal of Catalysis 158 (1996) 301–310.
[17] M. Devadas, O. Kröcher, M. Elsener, A. Wokaun, N. Söger, M. Pfeifer, Y. Demel, L. Mussmann, Applied Catalysis B: Environmental 67 (2006) 187–196.
[18] C. He, Y. Wang, Y. Cheng, C.K. Lambert, R.T. Yang, Applied Catalysis A: General 368 (2009) 121–126.
[19] T. Komatsu, M. Nunokawa, I.S. Moon, T. Takahara, S. Namba, T. Yashima, Journal of Catalysis 148 (1994) 427–437.
[20] J.-Y. Luo, X. Hou, P. Wijayakoon, S.J. Schmieg, W. Li, W.S. Epling, Applied Catalysis B: Environmental 102 (2011) 110–119.
[21] J. Girard, G. Cavataio, R. Snow, C. Lambert, SAE International Journal of Fuels and Lubricants 1 (2009) 603–610.
[22] R.M. Heck, Catalysis Today 53 (1999) 519–523.
[23] N.Y. Topsøe, Journal of Catalysis 128 (1991) 499–511.
[24] E.T.C. Vogt, A. Boot, A.J. van Dillen, J.W. Geus, F.J.J.G. Janssen, F.M.G. van den Kerkhof, Journal of Catalysis 114 (1988) 313–320.
[25] G. Cavataio, J. Girard, J.E. Patterson, C. Montreuil, Y. Cheng, C.K. Lambert, SAE Technical Paper 2007-01-1575, 2007, http://dx.doi.org/10.4271/2007-01-1575.
[26] E. Tronconi, I. Nova, C. Ciardelli, D. Chatterjee, B. Bandl-Konrad, T. Burkhardt, Catalysis Today 105 (2005) 529–536.
[27] I. Nova, C. Ciardelli, E. Tronconi, D. Chatterjee, B. Bandl-Konrad, AIChE Journal 52 (2006) 3222–3233.
[28] I. Nova, M. Colombo, E. Tronconi, V. Schmeisser, M. Weibel, SAE International Journal of Engines 4 (2011) 1822–1838.
[29] H. Sjövall, R.J. Blint, A. Gopinath, L. Olsson, Industrial and Engineering Chemistry Research 49 (2010) 39–52.
[30] L. Olsson, H. Sjövall, R.J. Blint, Applied Catalysis B: Environmental 81 (2008) 203–217.
[31] H. Sjövall, E. Fridell, R.J. Blint, L. Olsson, Topics in Catalysis 42–43 (2007) 113–117.
[32] H. Sjövall, L. Olsson, E. Fridell, R.J. Blint, Applied Catalysis B: Environmental 64 (2006) 180–188.
[33] N. Wilken, K. Kamasamudram, N.W. Currier, J. Li, A. Yezerets, L. Olsson, Catalysis Today 151 (2010) 237–243.
[34] K.W.N. Wilken, K. Kamasamudram, N.W. Currier, R. Vedaiyan, A. Yezerets, L. Olsson, Applied Catalysis B: Environmental 111–112 (2012) 58–66.
[35] J.-S. Choi, W.P. Partridge, C.S. Daw, Applied Catalysis A: General 293 (2005) 24–40.
[36] J.-S. Choi, W.P. Partridge, C.S. Daw, Applied Catalysis B: Environmental 77 (2007) 145–156.
[37] J.-S. Choi, W.P. Partridge, W.S. Epling, N.W. Currier, T.M. Yonushonis, Catalysis Today 114 (2006) 102–111.
[38] W.P. Partridge, J.-S. Choi, Applied Catalysis B: Environmental 91 (2009) 144–151.
[39] W.P. Partridge, T.J. Toops, J.B. Green, T.R. Armstrong, Journal of Power Sources 160 (2006) 454–461.
[40] K. Kamasamudram, N.W. Currier, X. Chen, A. Yezerets, Catalysis Today 151 (2010) 212–222.
[41] M. Koebel, G. Madia, M. Elsener, Catalysis Today 73 (2002) 239–247.
[42] P.S. Metkar, V. Balakotaiah, M.P. Harold, Catalysis Today 184 (2012) 115–128.
[43] G. Delahay, B. Coq, S. Kieger, B. Neveu, Catalysis Today 54 (1999) 431–438.
[44] G. Centi, S. Perathoner, D. Biglino, E. Giamello, Journal of Catalysis 152 (1995) 75–92.